

Communication

# An Electromagnetic–Thermal Coupling Numerical Study of the Synchronous Generator with Second-Generation High-Temperature Superconducting Armatures

Xiangyu Huang <sup>1</sup>, Zhen Huang <sup>1,\*</sup>, Xiaoyong Xu <sup>1</sup>, Wan Li <sup>2</sup> and Zhijian Jin <sup>1</sup>

<sup>1</sup> School of Electronic Information and Electrical Engineering, Shanghai Jiao Tong University, Shanghai 200240, China; huangxiangyu2014@sjtu.edu.cn (X.H.); xu\_xiaoyong@sjtu.edu.cn (X.X.); zjjin@sjtu.edu.cn (Z.J.)

<sup>2</sup> Shanghai Marine Equipment Research Institute, Shanghai 200031, China; liwan1699@126.com

\* Correspondence: zhen.huang@sjtu.edu.cn

Received: 2 July 2020; Accepted: 27 July 2020; Published: 29 July 2020



**Abstract:** Generators with high-temperature superconducting armatures have an advantage in the fact that they can carry high currents. However, the AC loss of high-temperature superconducting (HTS) armatures is difficult to calculate precisely because HTS coils exist in a complex and time-varying electromagnetic environment. In addition, when the HTS coil is carrying a short circuit fault overcurrent, an electromagnetic–thermal simulation study of this process is required to ensure that the HTS coil is not damaged. In this paper, first, a fully coupled T-A formulation model is used to calculate the AC loss of HTS armatures. Then, the current and temperature distributions are simulated, considering the intrinsic characteristic of superconducting coated conductors, when the generator suffers the worst short circuit fault accidentally. It is found that the turn with the lowest critical current quenches after 0.01 s, but the temperature rise cannot damage the coil if the circuit breaker can clear the fault quickly. The effects of the copper stabilizer thickness on the thermal stability of the HTS coil during the worst short circuit fault are also investigated. A thicker copper stabilizer improves the thermal stability of the HTS coil in the event of a short circuit fault, but the use of a simulation model is needed to make trade-offs between the engineering current density and the thermal stability of the HTS tapes. The work in this paper is necessary and can provide an important reference for manufacturing superconducting generators.

**Keywords:** AC loss; short circuit faults; T-A formulation; HTS generator

## 1. Introduction

Second-generation (2G) high-temperature superconducting (HTS) generators are promising because they can achieve a higher power density compared to conventional generators [1]. For synchronous generator applications, HTS coils placed in the stator have an advantage in terms of static cooling, but HTS coils will suffer AC loss because they are under alternating magnetic fields and currents.

The AC loss of an isolated HTS coil has been studied by many groups [2–6]. To calculate the AC loss of HTS coils in the actual generator environment, a two-stage segregated model consisting of a machine model and an AC loss model has been proposed [7] and used [8,9]. The rotating machine is first simulated by the A-formulation, and then the HTS coil is simulated by the H-formulation [10], with the boundary condition calculated from the A-formulation model.

The T-A formulation model [11,12] can fully couple the A-formulation model of the generator and the HTS coil model. The efficiency of the T-A formulation model is higher than the H-formulation

model due to the decrease in the degrees of freedom [11]. Moreover, the T-A formulation model can directly achieve the fully coupled simulation of the HTS coils under the generator's electromagnetic environment because rotating generators are usually simulated by the A-formulation [13].

When a short circuit fault happens, the magnetic field on the surface of the HTS coils and the current flowing in the coils will change drastically and cause a greater AC loss. The ohmic loss also occurs when the current exceeds the critical current of the coils. If the cooling capacity of the cryocooler is not enough to remove the heat immediately, the HTS coils may be permanently damaged [14]. To understand whether the short circuit fault will cause permanent damage to HTS coils, conducting an electromagnetic thermal coupling simulation is of great importance. It should be considered that these factors will have an effect on HTS materials, including the magnetic field, the current and the temperature.

To date, some numerical simulations of the short circuit faults of HTS generators have been done [15–19]. However, none of these simulations achieves fully coupled simulations, considering the dependence of the critical current density on the temperature and the magnetic field.

The main novelty of this paper is to conduct an electromagnetic–thermal coupling numerical study of a synchronous generator with 2G HTS armatures. In Section 2, the field–circuit thermal coupled model is introduced. In Section 3, the parameters of the HTS generator and the HTS coils are introduced. In Section 4, the model is first used to calculate the AC loss of the stator HTS coils under the rated condition of the generator. Then, the transient electromagnetic–thermal behavior of the HTS coils under a sudden three-phase short circuit fault at the no-load operation will be studied. This situation causes a maximum peak short circuit current, which is the worst case for the HTS coil. Moreover, the effects of the copper stabilizer thickness on the thermal stability of the HTS coil at the worst short circuit fault will also be investigated. Finally, our conclusions are drawn in Section 5.

## 2. Formulation and Model

To consider the complex anisotropy of YBCO tapes in our numerical model, the dependence of the critical current density on the magnetic flux density  $B$  and the temperature  $T$  is expressed as [4,20–22]:

$$J_c(B, T) = J_{c0} J_{cB}(B_{par}, B_{per}) J_{cT}(T) \quad (1)$$

$$J_{cB}(B_{par}, B_{per}) = \frac{1}{(1 + \sqrt{(kB_{par})^2 + B_{per}^2/B_c})^b} \quad (2)$$

$$J_{cT}(T) = J_c(T) = \begin{cases} \left(\frac{T_c - T}{T_c - T_0}\right) & T < T_c \\ 0 & T \geq T_c \end{cases} \quad (3)$$

where  $B_{par}$  and  $B_{per}$  represent the magnetic field component parallel and perpendicular to the tape surface, respectively.  $J_{c0}$  is the self-field critical current density at the operating temperature.  $b$ ,  $k$  and  $B_c$  are the curve-fitting parameters.  $T_c = 92$  K is the critical temperature.  $T_0 = 77$  K is the operating temperature.

It is important to note that Equations (2) and (3) are only an approximate expression of the dependence of the critical current density on the magnetic flux density and the temperature. The actual properties of the HTS tapes will not follow these expressions completely.

The superconducting layer resistivity is calculated by the E–J power law relation [23]:

$$\rho(J) = \frac{E_0}{J_c(B, T)} \left| \frac{J}{J_c(B, T)} \right|^{(n-1)} \quad (4)$$

where  $E_0$  is the critical electrical field, which is usually set as  $10^{-4}$  V/m.  $n$  is the critical exponent.

2.1. The Field Model

The current density vector potential  $T$  is defined in the superconducting layer to solve the current density distribution in HTS-coated conductors:

$$J = \nabla \times T \tag{5}$$

As can be seen in Figure 1, set the current density vector potential of the endpoint on one side of each HTS tape as zero, and the boundary condition for the 2-D T-formulation is:

$$I_{su} = \int_l J_z dl = \int_l -\frac{\partial T}{\partial y} dx = -(T_1 - T_2) = -T_1 \tag{6}$$

where  $I_{su}$  is the superconducting layer current of the HTS coil.

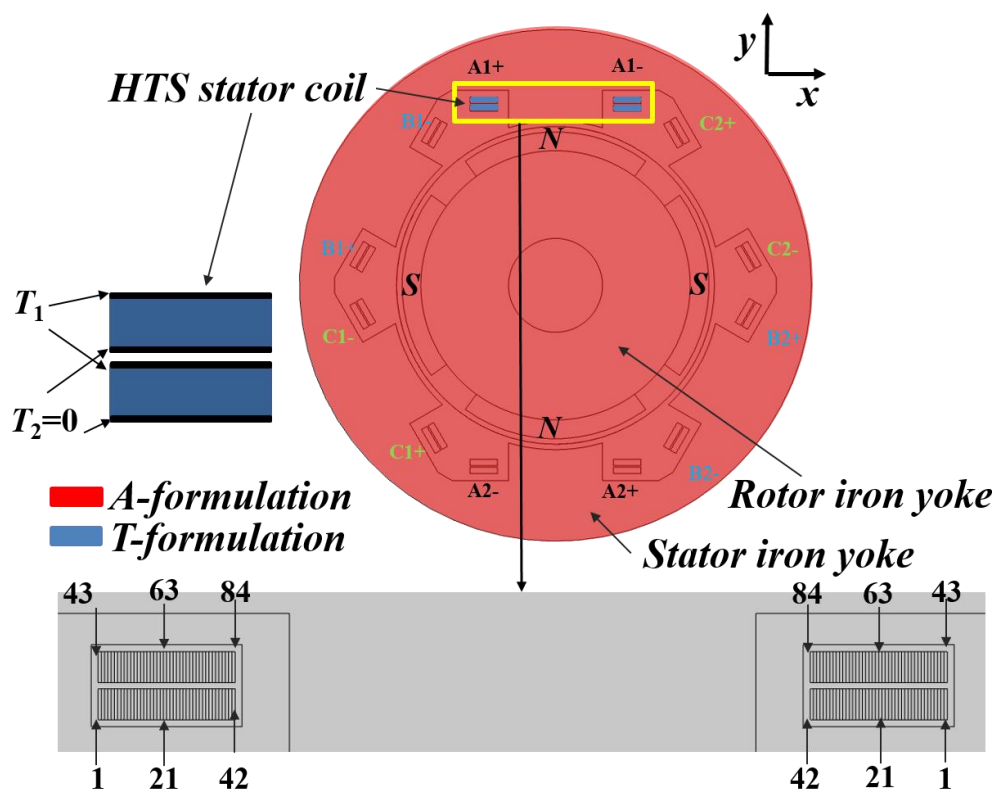


**Figure 1.** Schematic diagram for the 2-D T-A formulation, the topology of the generator and the numbering sequence of each turn of the studied coil.

In all domains of the generator, the magnetic vector potential  $A$  is defined and the A-formulation is used:

$$B = \nabla \times A \text{ all domains} \tag{7}$$

$$\frac{1}{\mu} \nabla \times (\nabla \times A) = \begin{cases} \nabla \times T & \text{superconducting layers} \\ J_{cu} & \text{copper layers} \end{cases} \tag{8}$$

$$-\frac{\partial A}{\partial t} = \rho(J) \nabla \times T \text{ superconducting layers} \tag{9}$$

where  $J_{cu}$  is the copper layer current density of the HTS coil, calculated by coupling with the circuit part (introduced in Section 2.2).  $\mu$  is the permeability of the material. The relative permeability for all the materials in the model is one.

The boundary condition for the A-formulation is set as:

$$A = 0 \tag{10}$$

### 2.2. The Circuit Model

The equivalent circuit model of the whole superconducting synchronous generator is shown in Figure 2. For the stator windings, since the three-phase stator windings are symmetrical, only the variables related to the phase-A winding are explained.

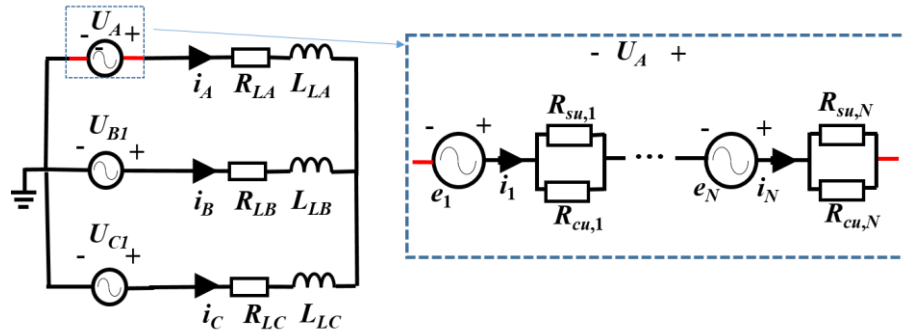


**Figure 2.** Schematic diagram for the equivalent circuit model of the high-temperature superconducting (HTS) generator.

The circuit equation of the phase-A is:

$$U_A = R_{LA}i_A + L_{LA} \frac{di_A}{dt} \tag{11}$$

where  $U_A$ ,  $L_{LA}$ ,  $R_{LA}$ ,  $i_A$  are the output voltage, the load inductance, the load resistance and the current of the phase-A winding, respectively.

For the HTS winding, it can be seen as a series of turns (right part of the Figure 2), and the circuit equations are [24]:

$$\begin{aligned}
 U_A &= \sum_{k=1}^N (e_k - i_k \frac{R_{su,k}R_{cu,k}}{R_{su,k} + R_{cu,k}}) \\
 e_k &= \frac{\int E_z dS}{S_k} L \\
 i_k &= i_{su,k} + i_{cu,k} \\
 R_{su,k} &= E_0 \frac{i_{su,k}^{n-1}}{I_c(B_{su,k}, T_{su,k})^n} l_k \\
 R_{cu,k} &= \frac{\rho_{cu}(T_{cu,k})l_k}{S_{cu,k}} \\
 R_{su,k}i_{su,k} &= R_{cu,k}i_{cu,k}
 \end{aligned} \tag{12}$$

where the subscript  $k$  represents the  $k$ -th turn of the HTS coil.  $N$  is the total number of turns of the coil.  $e_k$  is the generated electromotive force.  $E_z$  is the electric field strength in the coil domain.  $S_k$  is the cross-sectional area of the conductor.  $L$  is the core length.  $i_k$  is the total current.  $i$ ,  $R$  and  $T$  represent the current, the resistance and the temperature, respectively. The subscript  $su$  and  $cu$  represent the superconducting layer and copper layer, respectively.  $B_{su,k}$  is the magnetic flux density in the superconducting layer.  $l_k$  is the tape length.  $\rho_{cu}$  is the copper layer resistivity which is from [25].  $S_{cu,k}$  is the cross-section area of the copper layer.

### 2.3. The Thermal Model

The governing equation of the heat transfer model in the HTS coil is [25,26]:

$$dC \frac{\partial T}{\partial t} + \nabla \cdot (-k \nabla T) = Q_{su} + Q_{cu} \tag{13}$$

where  $d$ ,  $C$  and  $k$  are the mass density, the heat capacity and the thermal conductivity of the materials of each layer of the HTS coil, respectively. The material properties of the Kapton layer are from [26] and other layers are from [25].

The magnetization loss density  $Q_{su}$  is generated in the superconducting layers. The ohmic loss density  $Q_{cu}$  is generated in the copper layer, and it is caused by the shunting of the copper layer, which will occur after the total current exceeds the critical current of the HTS tapes.

The distribution of the same kind of loss in each turn is non-uniform because, in the current distribution, the magnetic field distribution and the temperature distribution of each turn are different. The values of these heat sources for each turn need to be calculated by coupling with the field model and the circuit model introduced previously:

$$Q_{su} = E(J)J \cdot J$$

$$Q_{cu,k} = \frac{i_{cu,k}^2 R_{cu,k}}{S_{cu,k} l_k} \tag{14}$$

During the operation of the HTS machine, the cryocooler will take away a certain amount of heat in coils. However, in order to estimate the most serious consequences of short circuit faults conservatively, the adiabatic boundary condition is set on the surface of the coils.

The coupling relationship among the field, circuit and thermal model of the HTS coils is summarized in Figure 3:

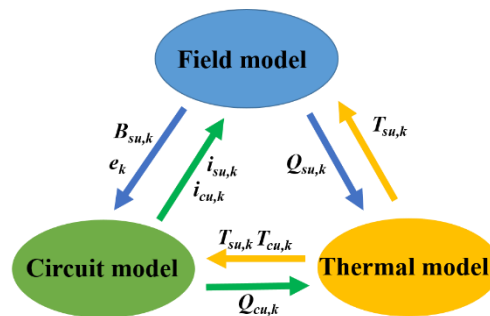


**Figure 3.** Schematic diagram for the coupling relationship among the field, circuit and thermal model.

The field model uses the temperature distribution calculated from the thermal model, and the current values of the superconducting layers and copper layers calculated from the circuit model, to calculate the magnetization loss of the superconducting layers, the magnetic field distribution, and the generated electromotive force of the HTS coils. The circuit model uses the temperature distribution calculated from the thermal model, and the magnetic field distribution calculated from the field model, to calculate the current values of the superconducting layers and copper layers and the copper layer loss.

All these models are implemented in the COMSOL Multiphysics software.

### 3. Parameters

The topology of the studied HTS generator is shown in Figure 1, each phase is composed of two coils in parallel. For example, the phase A winding consists of two coils: A1 and A2. A1+ and A1– are the positive current domain and the negative current domain of the A1 coil, respectively.

The studied generator has four poles and six slots. Each slot has one double racetrack coil with 84 turns. The rated current of these HTS field coils is about 37 A and the rated output power is 30 kW. The generator is designed to operate at 1500 rpm, corresponding to a stator armature frequency of 50 Hz.

Other design parameters for the generator can be found in a previous paper [27]. The parameters of the HTS coils are summarized in Table 1.  $b$ ,  $k$  and  $B_c$  are calculated by fitting the experimental data of a sample HTS tape. The surface plot of the normalized critical current density for the HTS tape under a parallel and perpendicular magnetic field is shown in Figure 4.

**Table 1.** Coil parameters.

Parameter	Value
Manufacturer	Shanghai Superconductor Technology
Superconducting layer material	ReBCO
Tape width	4 mm
Substrate layer material	Hastelloy
Copper stabilizer thickness	10 $\mu\text{m}$
$n$	28
Critical current of the tape (77 K, self-field)	135 A
$b$	1.058
$k$	0.0605
$B_c$	0.1942 T
Turns	84
Straight length of the coil	244 mm
Inner radius of the coil	37 mm

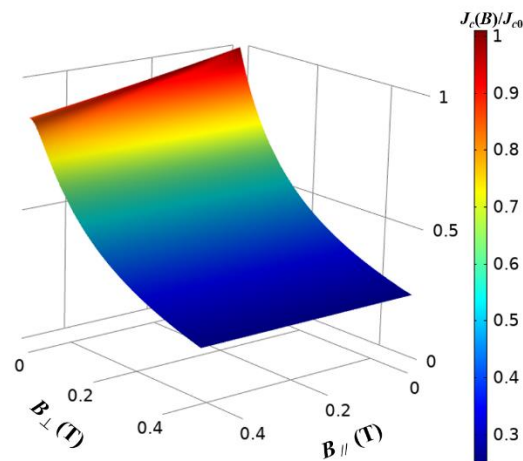


**Figure 4.** The surface plot of the normalized critical current density for the HTS tape under parallel and perpendicular magnetic field.

Since the six coils are symmetrical, only the results of the A1 coil are shown in this paper. The numbering sequence of each turn of the studied coil is shown in Figure 1, and this arrangement will be used throughout Section 4. Although this paper is only a numerical simulation study, it is worth mentioning that our group has now manufactured the stator of the generator, which is shown in Figure 5.

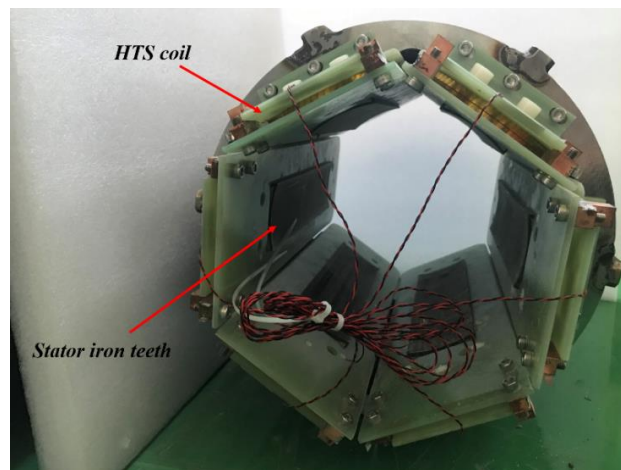


Figure 5. The manufactured generator stator.

#### 4. Results and Discussion

##### 4.1. AC Loss of HTS Coils under the Rated Operation

The induced AC loss on HTS armatures will directly affect the efficiency of the generator and thereby increase the cost of cooling. Hence, accurately and quickly estimating the AC loss of the HTS generator is urgent and beneficial. The T-A formulation model has offered a convenient tool to solve this problem. In this section, the AC loss of HTS coils in the generator during the rated operation will be calculated and discussed.

The calculated AC loss values of several representative turns, which are placed at different locations in the HTS coil, are summarized in Table 2. It can be seen that different turns of the coil have significantly different AC loss values. The calculated current waveform of the A1 coil in one cycle at the rated condition is shown in Figure 6, and four typical time moments, A, B, C and D, are chosen to show the calculation results.

Table 2. AC loss values of several representative turns.

Turn Number	AC Loss (W)
1	0.31
21	0.60
42	1.94
43	0.11
63	0.14
84	0.55

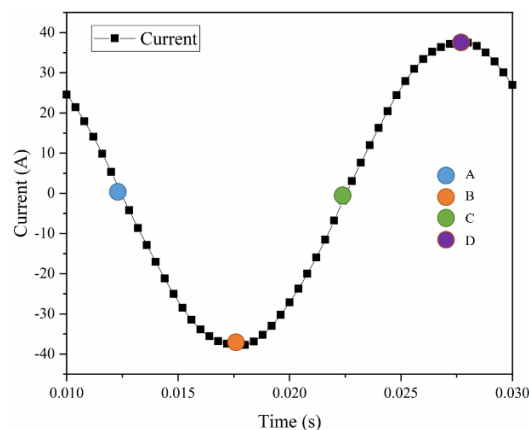
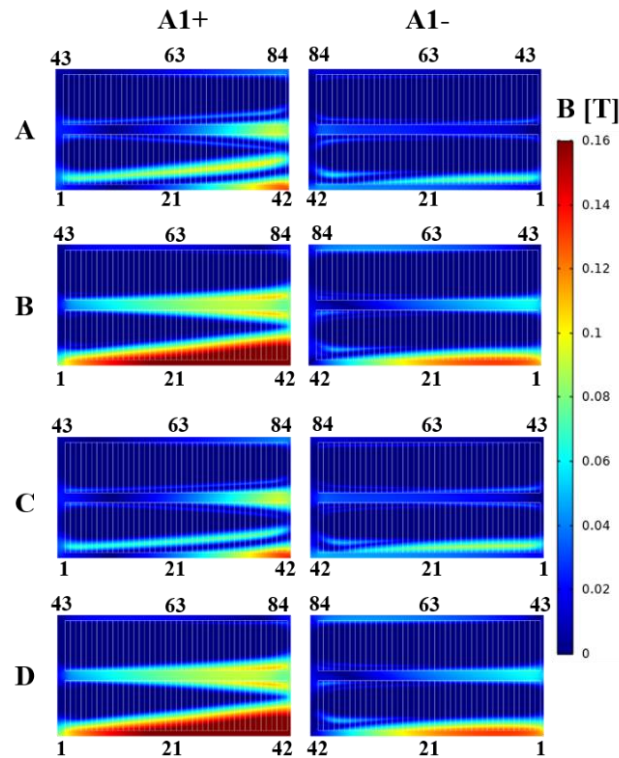


Figure 6. Current waveform of the studied A1 coil in one cycle.

The critical current of the HTS tapes is mainly influenced by the magnetic field perpendicular to the tape surface. Figure 7 shows the perpendicular magnetic flux density magnitude distributions of the area around the HTS tapes. First, due to the lower coil being closer to the rotor than the upper coil, its surface magnetic field is significantly larger than that of the upper coil. The turn in the lower coil has a greater AC loss value than the corresponding turn with the same distance to the stator iron teeth in the upper coil (e.g., turn 42 and turn 84). In addition, the perpendicular magnetic field in region A1+ is much greater than that in the A1− region. Although the average perpendicular magnetic field of turn 42 in the A1− region is less than turn 21, the average perpendicular magnetic field of turn 42 in the A1+ region is much greater than turn 21, which makes the AC loss of turn 42 greater than turn 21.



**Figure 7.** Perpendicular magnetic flux density magnitude distribution of the area containing the HTS tapes.

Figure 8 shows the normalized current density distribution of the HTS tapes. The normalized current density distribution is similar to the perpendicular magnetic field distribution. The critical current degradation is more severe in each turn of the lower coil due to the greater perpendicular magnetic field, so the current penetration into the interior of the HTS tapes is more severe, making the AC loss greater than the upper coil. Turn 42 in the lower coil suffers the maximum surface perpendicular magnetic field and has the minimum critical current because it is nearest to the iron teeth, which attracts the flux lines. Its current penetration is also the most severe and it has the greatest AC loss value.

The generator has three phases and is symmetrical. Since the current and magnetic field of each coil have three phases and are symmetrical, with only the phase angle being different, the AC loss is the same for all six coils. The calculated total AC loss of the 6 HTS coils is 229.38 W. Considering that the cooling penalty is about 10 [28], the loss ratio is about 5.29%.

#### 4.2. Transient Electromagnetic–Thermal Behavior of HTS Coils under the L-L-L Fault

In this section, the worst short circuit fault in the generator output terminal is studied: a sudden three-phase short circuit fault at the no-load operation. When a short circuit fault occurs at a time when

the electromotive force of the phase-A is passing through zero, the maximum fault current occurs in phase A [16], which is the worst scenario for the A1 HTS coil studied in this paper.

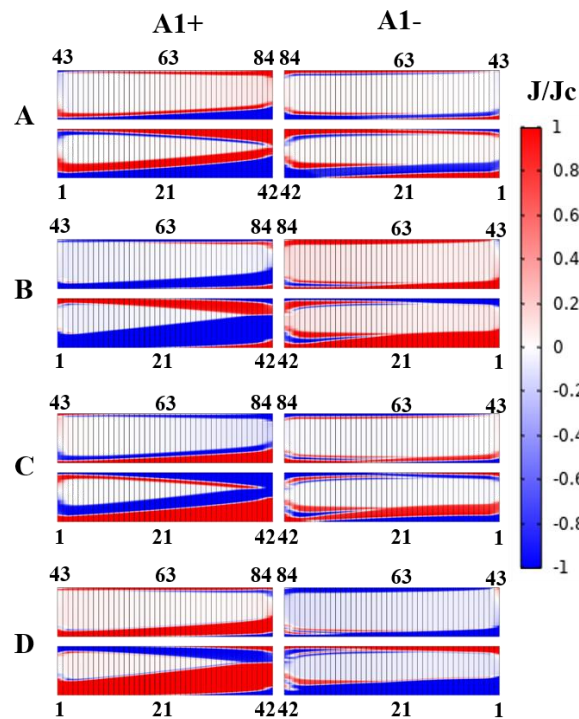


Figure 8. Normalized current density distribution of the HTS tapes.

When the fault happens, the generator short circuit fault protection system will act to cut off the fault current to remove the fault. Therefore, it is only necessary to pay attention to whether the short circuit fault will cause permanent harm to the superconducting coil within a short period of time after the fault occurs.

The short circuit fault occurs at  $t = 0.04$  s of the simulation and the circuit breaker can clear the fault in 0.08 s [17], which means that longer simulation is unnecessary. Figure 9 depicts the variations in the total current, the critical current (CC), the superconducting layer current (SLC) and the copper layer current (CLC) of turn 42 and turn 43 of the A1 coil before and after the occurrence of the worst short circuit fault. The scale of the  $x$ -axis has been changed to make it easier for the reader to observe the waveform at 0.04–0.06 s. Figure 10 depicts the variations in the ohmic loss values and temperature values of turn 42 and turn 43 after the occurrence of the worst short circuit fault.

Turn 42 and turn 43 are chosen because the former has the lowest critical current and the most obvious temperature rise in each turn of the coil, while the latter has the highest critical current. As will be shown below, although the total current is the same for both them, during a short circuit fault, due to their different magnetic field environments, their critical current values are different. This difference in the critical current values at the beginning results in their different subsequent copper layer shunting and temperature rise phenomena in each HTS tape.

It can be clearly found that the total current increases rapidly after the occurrence of the short circuit fault. The critical current of turn 42 is much lower than that of turn 43 because of the different magnetic field environments on their surfaces. When the total current first exceeds the CC of turn 42 (0.0428 s), the excess current flows through the copper layer, producing the ohmic loss and raising the temperature. However, turn 43 is still in the superconducting state. As the short circuit current increases further, the total current exceeds the CC of turn 43 (0.0436 s); due to its high critical current, the copper layer current of turn 43 is less than turn 42's, resulting in less ohmic loss and a lower temperature rise.

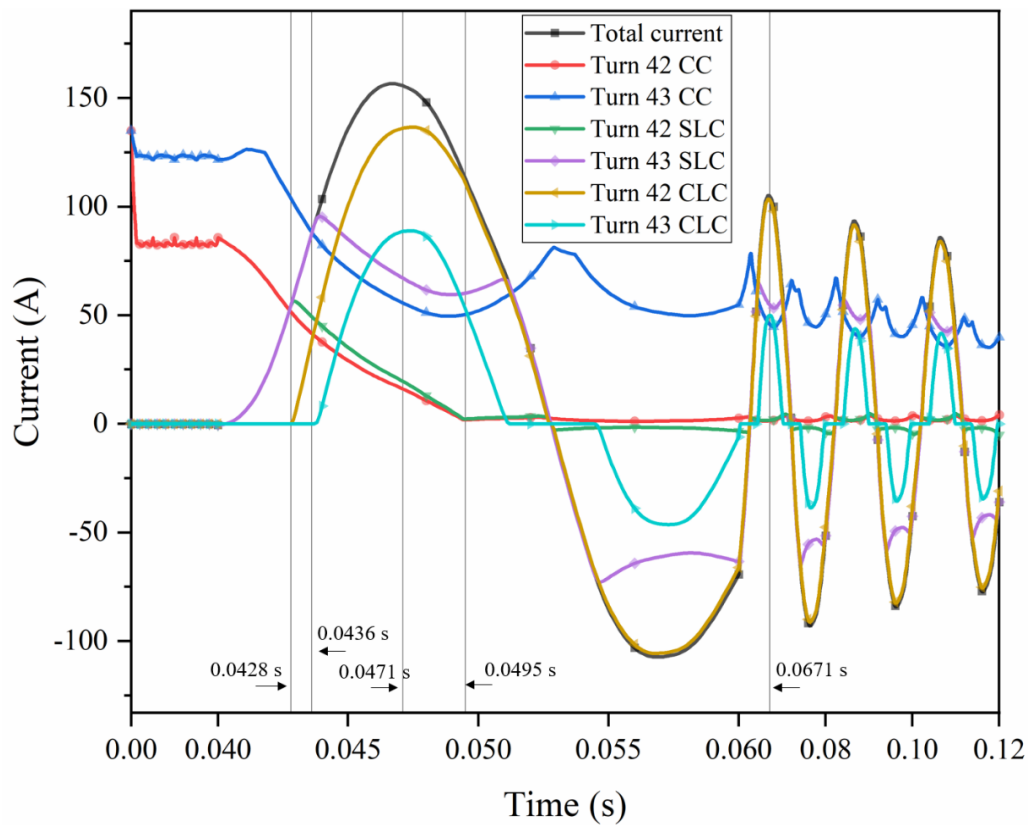


**Figure 9.** Waveforms of the total current, the critical current (CC), the superconducting layer current (SLC) and the copper layer current (CLC) of turn 42 and turn 43 before and after the occurrence of the worst short circuit fault.

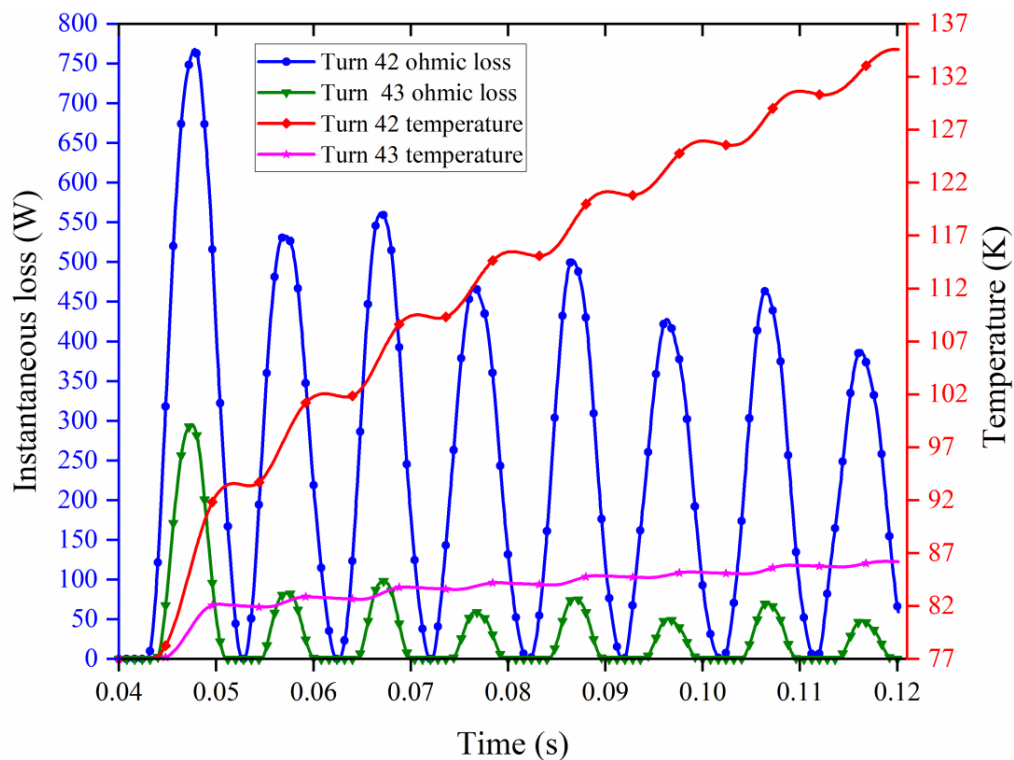


**Figure 10.** Waveforms of the ohmic loss values and the temperature values of turn 42 and turn 43 after the occurrence of the worst short circuit fault.

For turn 43, due to the non-periodic current component in the short circuit transient process, a peak value (0.0471 s) appears in the first half-cycle after the short circuit fault happens. With this component gradually decaying to zero, the waveform will eventually stabilize into a steady state. Since there is not much of a temperature rise for turn 43 after the first and also the highest peak current (0.0471 s), the subsequent smaller current peaks (for example, the 0.0671 s moment) also cannot induce much of a temperature rise in turn 43.

As for turn 42, after the 0.0471 s moment, although the total current is decreasing, the CC is still decreasing as well and the CLC can still increase for a short time. This phenomenon is caused by the temperature rise due to the ohmic loss. The higher temperature means lower CC, making the copper layer shunt phenomenon more severe and accelerating the temperature rise. After the 0.0495 s moment, the temperature of turn 42 rises to the critical temperature. Turn 42 loses its superconducting characteristic, and all the short circuit currents go through the copper layer.

A large amount of ohmic loss in a short time may cause damage to the HTS coil and this phenomenon is worthy of vigilance. One solution is to design a HTS coil with a greater margin to get through the short time overcurrent process. However, this method is not economical. Another method is to allow the current to exceed the critical current value in a short time as long as the temperature rise is limited and the HTS coil can return to the superconducting state after the fault disappears [29].

For the whole HTS coil, although the temperature rise in the turn with the lowest critical current is obvious, the highest temperature at  $t = 0.12$  s is not high enough to exceed the melting points of the materials of the HTS coil. As long as the machine short circuit protection device can remove the fault, the HTS coil will not be damaged.

#### *4.3. Effects of the Copper Stabilizer Thickness on the Thermal Stability of the HTS Coil*

Copper stabilizer can improve the thermal stability of the 2G HTS tapes [30]. In this section, the effects of the copper stabilizer thickness on the thermal stability of the HTS coil during the worst short circuit fault are numerically studied.

Figure 11 depicts the variations in the total current, the critical current and the copper layer current of turn 42 after the occurrence of the worst short circuit fault, with copper stabilizer thicknesses of 10  $\mu\text{m}$  and 20  $\mu\text{m}$ . Figure 12 depicts the ohmic loss values and the temperature values of turn 42 after the occurrence of the worst short circuit fault with copper stabilizer thicknesses of 10  $\mu\text{m}$  and 20  $\mu\text{m}$ .

It is found that, as the copper stabilizer thickens, the temperature rise phenomenon becomes weaker. The temperature rise in the copper layer in a short period can be approximately considered to be proportional to the ohmic loss volume density (ignore the heat transfer from the copper layer to other layers to simplify the explanation). The ohmic loss volume density is proportional to the square of the current density of the copper layer, so the temperature rise in the copper layer can be approximately regarded as inversely proportional to the square of the thickness of the copper stabilizer. Thus, although the time when the total current exceeds the critical current is almost the same for the two cases, the final temperature will be lower for the thicker copper stabilizer.

However, though the thicker copper stabilizer improves the thermal stability of the HTS coil in the event of a short circuit fault, the engineering current density also decreases. For the HTS generator designer, this requires the use of an electromagnetic–thermal coupling numerical simulation model to make trade-offs between the engineering current density and the thermal stability of the HTS tapes.

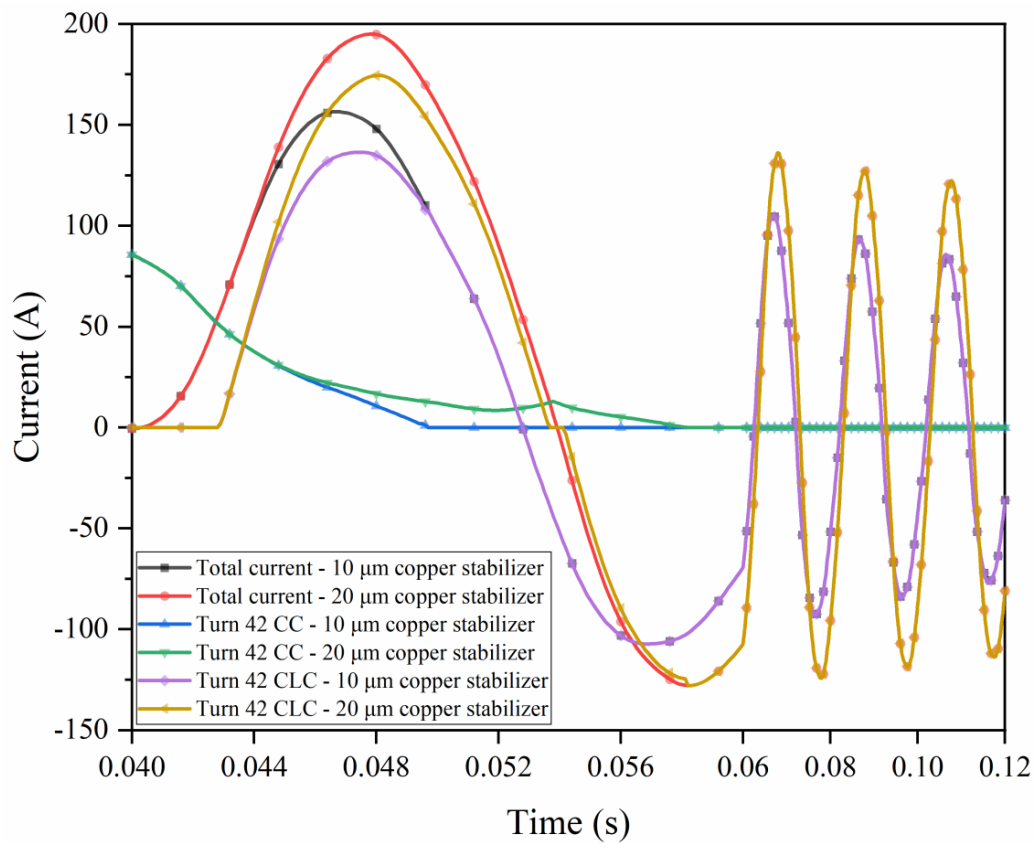


**Figure 11.** Waveforms of the total current, the critical current (CC), the superconducting layer current (SLC) and the copper layer current (CLC) of turn 42 after the occurrence of the worst short circuit fault with copper stabilizer thicknesses of 10  $\mu\text{m}$  and 20  $\mu\text{m}$ .

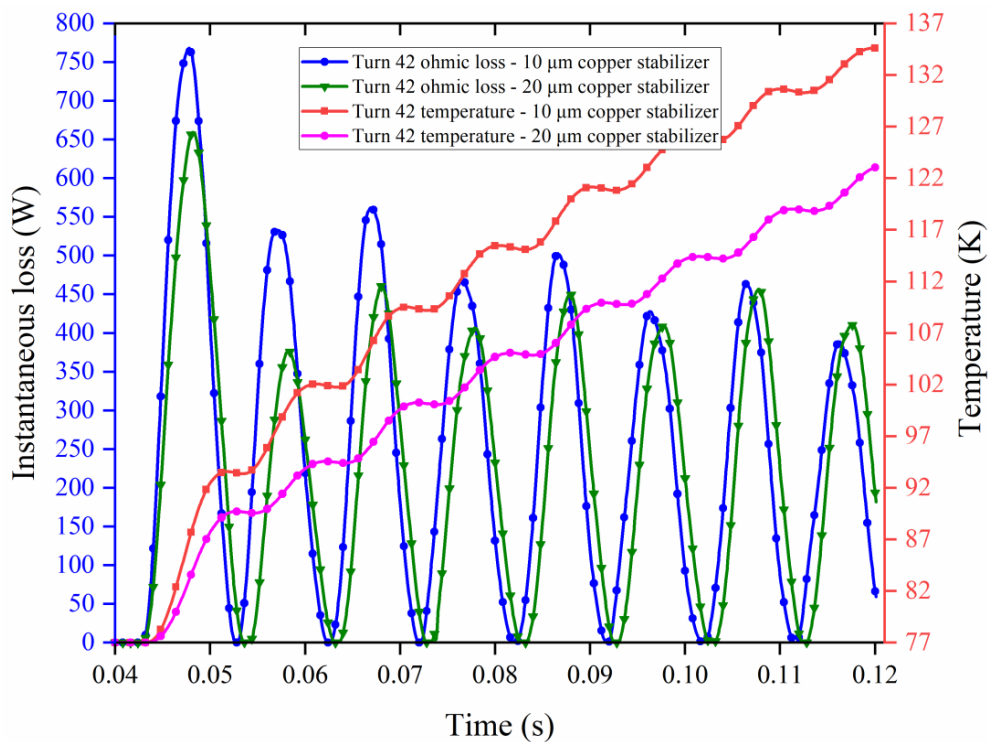


**Figure 12.** Waveforms of the ohmic loss values and the temperature values of turn 42 after the occurrence of the worst short circuit fault with copper stabilizer thicknesses of 10  $\mu\text{m}$  and 20  $\mu\text{m}$ .

One noteworthy phenomenon is that the total current eventually becomes inconsistent after a short circuit fault occurs in both cases. The total current in both cases is the same at the beginning of the short circuit fault because the coil is initially in the superconducting state and the coil resistance is almost zero. The short circuit impedance is mainly the inductive resistance of the coil, which is the same for the two cases. Then, as the temperature rises, the coil resistance is gradually dominated by the copper layer resistance and the short circuit impedance becomes greater. For the thicker copper stabilizer case, the copper layer resistance is smaller, so the short circuit impedance is smaller, causing a greater short circuit current. Moreover, since the copper layer loss is proportional to the square of the current, finally, at  $t = 0.12$  s, the 20- $\mu\text{m}$  copper stabilizer case's ohmic loss even exceeds that of the 10- $\mu\text{m}$  copper stabilizer case by a little.

## 5. Conclusions

In this paper, an electromagnetic–thermal coupling numerical study of a synchronous generator with 2G HTS armatures is conducted. The main results in this paper are summarized as follows:

First, by coupling the field part model with the circuit part model, the AC loss of HTS coils during rated operation is calculated. Second, the transient electromagnetic–thermal behavior of the HTS coil under the worst short circuit fault is studied. The results show that although the total current is the same for each turn of the HTS coil during the short circuit fault, the critical current value of each turn is different due to their diverse surrounding magnetic fields. This difference in the critical current value at the beginning leads to their subsequently different copper layer shunting and temperature rise phenomena. The turn with the lowest critical current will eventually quench completely, and the temperature rise is obvious, but it is not high enough to exceed the melting points of the materials of the HTS coil. It is concluded from this work that, if the generator short circuit protection device can remove the fault as soon as possible, the HTS coil in this high-speed HTS synchronous generator will not suffer unrecoverable quench and be damaged. Last but not least, the simulation results show that a thicker copper stabilizer improves the thermal stability of the HTS coil in the event of a short circuit fault, but for the HTS generator designer, this requires the use of a simulation model to make trade-offs between the engineering current density and the thermal stability of the HTS tapes.

**Author Contributions:** Conceptualization, X.H.; methodology, X.H.; investigation, W.L.; writing—original draft preparation, X.X.; writing—review and editing, Z.H.; supervision, Z.J. All authors have read and agreed to the published version of the manuscript.

**Funding:** This research was funded by the National Natural Science Foundation of China (Project No. 51707120), the Shanghai Rising-Star Program (20QC1401400) and the Shanghai Marine Equipment Research Institute (Project No. 18H100000488).

**Conflicts of Interest:** The authors declare no conflict of interest.

## References

1. Barnes, P.N.; Sumption, M.D.; Rhoads, G.L. Review of High Power Density Superconducting Generators: Present State and Prospects for Incorporating YBCO Windings. *Cryogenics* **2005**, *45*, 670–686. [[CrossRef](#)]
2. Chen, Y.; Zhang, M.; Chudy, M.; Matsuda, K.; Coombs, T. Complex Study of Transport AC Loss in Various 2G HTS Racetrack Coils. *Phys. C Supercond.* **2013**, *487*, 31–36. [[CrossRef](#)]
3. Zermeno, V.M.R.; Abrahamsen, A.B.; Mijatovic, N.; Jensen, B.B.; Sørensen, M.P. Calculation of Alternating Current Losses in Stacks and Coils Made of Second Generation High Temperature Superconducting Tapes for Large Scale Applications. *J. Appl. Phys.* **2013**, *114*, 173901. [[CrossRef](#)]
4. Wang, Y.; Zhang, M.; Grilli, F.; Zhu, Z.; Yuan, W. Study of the Magnetization Loss of CORC<sup>®</sup> Cables Using a 3D T-A Formulation. *Supercond. Sci. Technol.* **2019**, *32*, 025003. [[CrossRef](#)]
5. Zhang, M.; Yuan, W.; Kvitkovic, J.; Pamidi, S. Total AC Loss Study of 2G HTS Coils for Fully HTS Machine Applications. *Supercond. Sci. Technol.* **2015**, *28*, 115011. [[CrossRef](#)]
6. Liu, G.; Zhang, G.; Jing, L.; Ai, L.; Yu, H.; Li, W.; Liu, Q. Study on the AC Loss Reduction of REBCO Double Pancake Coil. *IEEE Trans. Appl. Supercond.* **2018**, *28*, 1–6. [[CrossRef](#)]

7. Zermeno, V.M.R.; Abrahamsen, A.B.; Mijatovic, N.; Sorensen, M.P.; Jensen, B.B.; Pedersen, N.F. Simulation of an HTS Synchronous Superconducting Generator. *Phys. Procedia* **2012**, *36*, 786–790. [CrossRef]
8. Song, X.; Mijatovic, N.; Zou, S.; Jensen, B.B.; Holboll, J. AC Losses and Their Thermal Effect in High-Temperature Superconducting Machines. *IEEE Trans. Appl. Supercond.* **2016**, *26*, 1–5. [CrossRef]
9. Li, Y.; Feng, F.; Li, Y.; Song, P.; Zou, S.; Wu, M.; Gu, C.; Zeng, P.; Qu, T. Numerical Study on AC Loss Characteristics of REBCO Armature Windings in a 15-KW Class Fully HTS Generator. *IEEE Trans. Appl. Supercond.* **2017**, *27*, 1–6. [CrossRef]
10. Hong, Z.; Campbell, A.M.; Coombs, T.A. Numerical Solution of Critical State in Superconductivity by Finite Element Software. *Supercond. Sci. Technol.* **2006**, *19*, 1246–1252. [CrossRef]
11. Zhang, H.; Zhang, M.; Yuan, W. An Efficient 3D Finite Element Method Model Based on the T–A Formulation for Superconducting Coated Conductors. *Supercond. Sci. Technol.* **2017**, *30*, 024005. [CrossRef]
12. Liang, F.; Venuturumilli, S.; Zhang, H.; Zhang, M.; Kvitkovic, J.; Pamidi, S.; Wang, Y.; Yuan, W. A Finite Element Model for Simulating Second Generation High Temperature Superconducting Coils/Stacks with Large Number of Turns. *J. Appl. Phys.* **2017**, *122*, 043903. [CrossRef]
13. Ainslie, M.; Grilli, F.; Queval, L.; Pardo, E.; Perez-Mendez, F.; Mataira, R.; Morandi, A.; Ghabeli, A.; Bumby, C.; Brambilla, R. A New Benchmark for Electromagnetic Modelling of Superconductors: The High-Tc Superconducting Dynamo. *arXiv* **2020**, arXiv:physics/219966041. Available online: <https://www.semanticscholar.org/paper/A-new-benchmark-for-electromagnetic-modelling-of-Ainslie-Grilli/4660781a5fc2c1706fe40bd437e632b46ed52c6d> (accessed on 2 July 2020).
14. Song, X.; Liu, D.; Polinder, H.; Mijatovic, N.; Holboll, J.; Jensen, B.B. Short Circuits of a 10-MW High-Temperature Superconducting Wind Turbine Generator. *IEEE Trans. Appl. Supercond.* **2017**, *27*, 1–5. [CrossRef]
15. Liu, Y.; Qu, R.; Wang, J.; Fang, H.; Zhang, X.; Chen, H. Influences of Generator Parameters on Fault Current and Torque in a Large-Scale Superconducting Wind Generator. *IEEE Trans. Appl. Supercond.* **2015**, *25*, 1–9. [CrossRef]
16. Huang, Z.; Zhao, A.; Huang, X.; Zhu, B.; Jiang, Y.; Jin, Z. Short-Circuit Fault Simulations in an HTS Wind Generator with Different Mechanical Conditions. *IEEE Trans. Appl. Supercond.* **2018**, *28*, 1–6. [CrossRef]
17. Vedreno-Santos, F.; Guan, Y.; Azar, Z.; Thomas, A.S.; Li, G.J.; Odavic, M.; Zhu, Z.Q. Comparison of Peak Armature and Field Winding Currents for Different Topologies of 10-MW Superconducting Generators Under Short-Circuit Conditions. *IEEE Trans. Appl. Supercond.* **2016**, *26*, 1–7. [CrossRef]
18. Guan, Y.; Vedreño-Santos, F.; Azar, Z.; Thomas, A.S.; Li, G.-J.; Odavic, M.; Zhu, Z.-Q. Performance of Superconducting Generators with Different Topologies under Fault Conditions. *J. Eng.* **2019**, *2019*, 4090–4095. [CrossRef]
19. Liu, D.; Polinder, H.; Abrahamsen, A.B.; Ferreira, J.A. Effects of an Electromagnetic Shield and Armature Teeth on the Short-Circuit Performance of a Direct Drive Superconducting Generator for 10 MW Wind Turbines. In Proceedings of the 2015 IEEE International Electric Machines & Drives Conference (IEMDC), IEEE, Coeur d’Alene, ID, USA, 10–13 May 2015; pp. 709–714. [CrossRef]
20. Grilli, F.; Sirois, F.; Zermeno, V.M.R.; Vojenciak, M. Self-Consistent Modeling of the  $J_c$  of HTS Devices: How Accurate Do Models Really Need to Be? *IEEE Trans. Appl. Supercond.* **2014**, *24*, 1–8. [CrossRef]
21. Song, M.; Li, L.; Wang, M.; Zhong, L.; Duan, X.; Li, Z.; Dong, F.; Yao, L.; Hong, Z.; Jin, Z. Numerical Study on Lightning Current Performance of Striated YBCO-Coated Conductor. *IEEE Trans. Appl. Supercond.* **2019**, *29*, 1–5. [CrossRef]
22. Zhang, J.W.; Hu, D.; Zhang, L.; Song, M.; Luo, Y.S.; Li, L.; Feng, G.; Li, Z.Y.; Hong, Z.; Jin, Z. Numerical Study of the Thermal Stability of YBa<sub>2</sub>Cu<sub>3</sub>O<sub>7- $\delta$</sub>  Tapes Suffering Lightning Current. *IEEE Trans. Appl. Supercond.* **2018**, *28*, 1–7. [CrossRef]
23. Rhyner, J. Magnetic Properties and AC-Losses of Superconductors with Power Law Current–Voltage Characteristics. *Phys. C Supercond.* **1993**, *212*, 292–300. [CrossRef]
24. Liu, D.; Yong, H.; Zhou, Y. Analysis of Charging and Sudden-Discharging Characteristics of No-Insulation REBCO Coil Using an Electromagnetic Coupling Model. *AIP Adv.* **2017**, *7*, 115104. [CrossRef]
25. Casali, M.; Breschi, M.; Ribani, P.L. Two-Dimensional Anisotropic Model of YBCO Coated Conductors. *IEEE Trans. Appl. Supercond.* **2015**, *25*, 1–12. [CrossRef]

26. Zhang, M.; Matsuda, K.; Coombs, T.A. New Application of Temperature-Dependent Modelling of High Temperature Superconductors: Quench Propagation and Pulse Magnetization. *J. Appl. Phys.* **2012**, *112*, 043912. [[CrossRef](#)]
27. Xu, X.; Huang, Z.; Li, W.; Dong, F.; Hao, L.; Shen, B.; Jin, Z. Study on Reducing the Maximum Perpendicular Magnetic Field of HTS Coils Used on Synchronous Generator Armatures. *IEEE Trans. Appl. Supercond.* **2019**, *29*, 1–5. [[CrossRef](#)]
28. Iwasa, Y. *Case Studies in Superconducting Magnets: Design and Operational Issues*, 2nd ed.; Springer: New York, NY, USA, 2009; p. 227.
29. Sivasubramaniam, K.; Huang, X.; Laskaris, E.T.; Zhang, T.; Bray, J.W.; Forgarty, J.M.; Nold, R.A. Performance of an HTS Generator Field Coil Under System Fault Conditions. *IEEE Trans. Appl. Supercond.* **2006**, *16*, 1971–1975. [[CrossRef](#)]
30. Kim, H.M.; Jankowski, J.; Lee, H.; Bascunan, J.; Fleshler, S.; Iwasa, Y. Stability of Bare and Copper-Laminated YBCO Samples: Experimental & Simulation Results. *IEEE Trans. Appl. Supercond.* **2004**, *14*, 1290–1293. [[CrossRef](#)]



© 2020 by the authors. Licensee MDPI, Basel, Switzerland. This article is an open access article distributed under the terms and conditions of the Creative Commons Attribution (CC BY) license (<http://creativecommons.org/licenses/by/4.0/>).